bioRxiv preprint doi: https://doi.org/10.1101/2021.02.16.431182; this version posted February 17, 2021. The copyright holder for this preprint (which was not certified by peer review) is the author/funder. All rights reserved. No reuse allowed without permission.

Similar neural and perceptual masking effects of low-power optogenetic stimulation in primate V1

Spencer Chen[1,2,3,10], Giacomo Benvenuti[1,2,3], Yuzhi Chen[1,2,3], Satwant Kumar[1,2,3], Charu Ramakrishnan[6], Karl Deisseroth[5,6,7,8,9], Wilson S. Geisler[1,2,4], Eyal Seidemann[1,2,3,4,11*]

[1]Center for Perceptual Systems, University of Texas, Austin, TX 78712, USA

[2]Department of Psychology, University of Texas, Austin, TX 78712, USA

[3]Department of Neuroscience, University of Texas, Austin, TX 78712, USA

[4]Neurosciences Program, University of Texas, Austin, TX 78712, USA

[5]Department of Bioengineering, Stanford University, Stanford, CA 94305, USA

[6]CNC Program, Stanford University, Stanford, CA 94304, USA

[7]Neurosciences Program, Stanford University, Stanford, CA 94305, USA

[8]Department of Psychiatry and Behavioral Sciences, Stanford University, Stanford, CA 94305, USA

[9]Howard Hughes Medical Institute, Stanford University, Stanford, CA 94305, USA

[10]Department of Neurosurgery, Rutgers University, New Brunswick, NJ 08901, USA

[11]Lead Contact

[*]Correspondence: eyal@austin.utexas.edu

bioRxiv preprint doi: https://doi.org/10.1101/2021.02.16.431182; this version posted February 17, 2021. The copyright holder for this preprint (which was not certified by peer review) is the author/funder. All rights reserved. No reuse allowed without permission.

Abstract

Can direct stimulation of primate V1 substitute for a visual stimulus and mimic its perceptual effect? To address this question, we developed an optical-genetic toolkit to "read" neural population responses using widefield calcium imaging, while simultaneously using optogenetics to "write" neural responses into V1 of behaving macaques. We focused on the phenomenon of visual masking, where detection of a dim target is significantly reduced by a co-localized medium-brightness pedestal. Using our toolkit, we tested whether V1 optogenetic stimulation can recapitulate the perceptual masking effect of a visual pedestal. We find that, similar to a visual pedestal, low-power optostimulation can significantly reduce visual detection sensitivity, that a sublinear interaction between visual and optogenetic evoked V1 responses could account for this perceptual effect, and that these neural and behavioral effects are spatially selective. Our toolkit and results open the door for further exploration of perceptual substitutions by direct stimulation of sensory cortex.

Introduction

A central goal of sensory neuroscience, and a prerequisite for the development of effective sensory cortical neuroprostheses, is to understand the nature of the neural code – that is, to determine which patterns of neural activity in early sensory cortex are necessary and sufficient in order to elicit a given percept. A promising experimental paradigm for testing specific hypotheses regarding the neural code is to use optogenetic stimulation (optostim) to directly insert neural signals into sensory cortex of alert, behaving animals. By using concomitant optical imaging of genetically encoded calcium indicators, one can measure the impact of these inserted signals on cortical circuits, calibrate the evoked neural population responses, and compare them to those evoked by sensory stimuli. Finally, by carefully

bioRxiv preprint doi: https://doi.org/10.1101/2021.02.16.431182; this version posted February 17, 2021. The copyright holder for this preprint (which was not certified by peer review) is the author/funder. All rights reserved. No reuse allowed without permission.

monitoring behavior while animals perform demanding sensory tasks, the perceptual consequences of these inserted signals can be assessed and compared with theoretical predictions.

This powerful experimental approach for all-optical interrogation of sensory cortex has recently been successfully used to study the neural code in rodents (e.g., [1-3]). However, the merging of optostim and optical imaging of calcium signals in behaving non-human primates (NHPs), a powerful animal model for studying human perception, is still in its infancy [4], and multiple barriers remain before this approach can be used routinely in NHPs [5-7]. For example, while optostim in early sensory cortex has been demonstrated to cause clear neural (e.g., [4, 8-12]) and behavioral (e.g., [4, 10-12]) effects in NHPs, such experiments typically require high-power optostimulation (10s to 100s of mW/mm^2) , and the evoked neural responses are typically monitored by electrophysiology which only captures a small fraction of the optostim-triggered neural population response.

To overcome some of these barriers, we have been working to develop a bi-directional optical-genetic toolkit for measuring ("reading") and modulating ("writing") neural population responses in behaving macaque cortex (**Fig. 1A**). First, we developed viral-based methods for stable long-term co-expression of a calcium indicator (GCaMP6f; [13]) and a red-shifted opsin (C1V1; [14]) in a population of excitatory V1 neurons (**Fig. 2A**). Second, we developed a widefield imaging system that allows us to simultaneously optostimulate and image NHP cortex with negligible cross-talk between these optical read/write components (**Fig. 2B**).

bioRxiv preprint doi: https://doi.org/10.1101/2021.02.16.431182; this version posted February 17, 2021. The copyright holder for this preprint (which was not certified by peer review) is the author/funder. All rights reserved. No reuse allowed without permission.

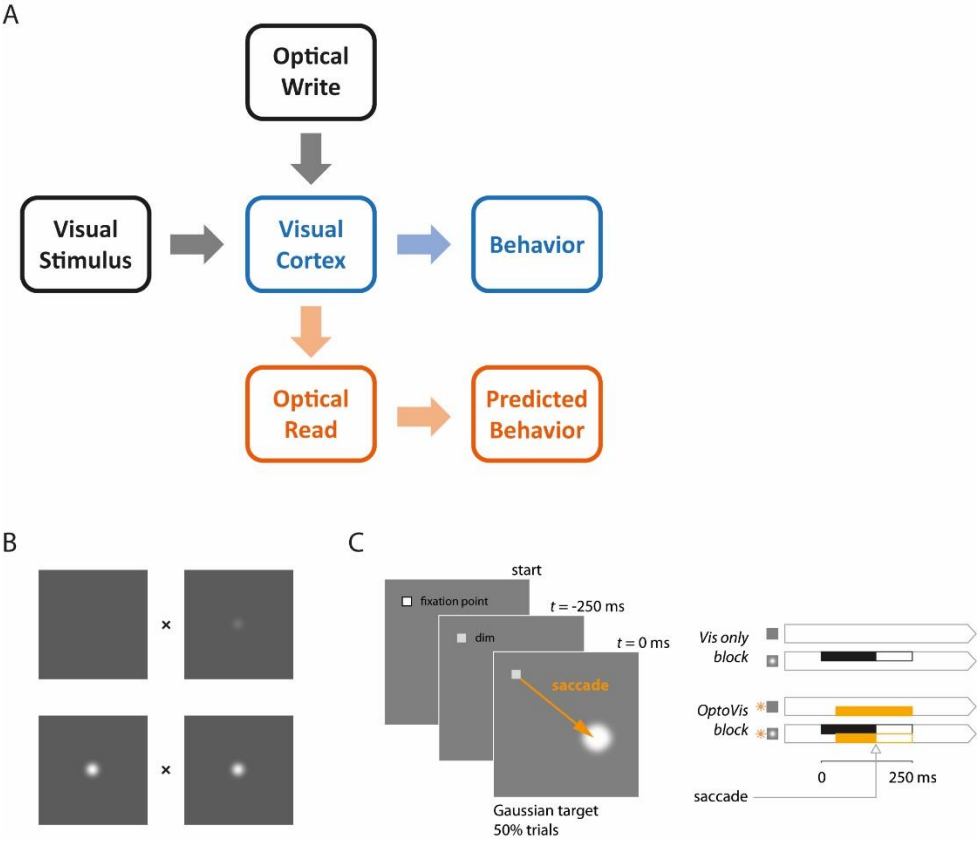

Figure 1. A general framework for bi-directional optical-genetic probing of the visual cortex in behaving monkeys, a demonstration of visual masking and a detection task for probing the masking effect of V1 optostimulation. (A) General framework. Our optical-genetic toolkit allows us to provide the subject with two types of inputs either separately or in combination: (i) visual ("Visual Stimulus") and (ii) direct optostimulation ("Optical Write"). At the same time, we have access to two outputs: (i) neural responses measured by widefield optical imaging ("optical read") and (ii) behavioral responses ("behavior"). Imaging allows us to measure the neural impact of the inserted signals, calibrate the evoked neural population responses, and compare them to those evoked by sensory stimuli. Finally, the neural and perceptual consequences of these inserted signals can be assessed and compared with theoretical predictions. Here we use this toolkit to measure the interactions between visual and direct optostimulation in macaque V1. **(B)** Demonstration of visual masking. When fixating on the x between the pair of panels, a visual target (a dim white Gaussian) can be easily detected when added to a uniform gray background (top), but is much harder to detect when added to a Gaussian pedestal (bottom), a phenomenon known as luminance masking. The goal of the current study was to determine whether direct optogenetic stimulation of V1 can substitute

bioRxiv preprint doi: https://doi.org/10.1101/2021.02.16.431182; this version posted February 17, 2021. The copyright holder for this preprint (which was not certified by peer review) is the author/funder. All rights reserved. No reuse allowed without permission.

for a visual pedestal and elevate detection threshold of a visual target. **(C)** The behavioral task adopted to quantify the masking effects of optostimulation. Two monkeys were trained to detect a small white Gaussian target that appeared 250 ms after a temporal cue (dimming of the fixation point) in half of the trials. The monkeys indicated target absence by maintaining fixation at the fixation point and target presence by shifting gaze to the target location as soon as it was detected. The visual target was present for a maximum of 250 ms and was terminated as soon as the monkey initiated a saccade. The optostim was initiated 40 ms after the expected time of target onset (to account for the latency of V1 responses) and was terminated together with the visual stimulus. Blocks of trials without optostim (right top) and with optostim (right bottom) were run separately. In optostim blocks, optostim (orange) was applied *on every trial,* acting as a substitute for the visual pedestal in **B**. The monkeys were always rewarded based on the presence or absence of the visual target only (right panels, black), irrespective of the optostim condition (orange). Note: in the bottom panels of **B** the target was added on the left.

Our long-term goal is to use this toolkit to study the nature of the neural code by testing the extent to which one can substitute visual stimulation with direct optostim in a behaving NHP that is engaged in a demanding perceptual task. Previous pioneering studies using electrical microstimulation in area MT of macaques performing a random-dot direction discrimination task demonstrated that microstimulation at the center of a direction selective MT column can substitute for a visual motion signal and strongly bias perceptual reports in favor of the direction preferred by the stimulated neurons [15, 16]. An important feature of these experiments was that monkeys were always rewarded for reporting the direction of motion of the visual stimulus irrespective of the microstimulation. The finding that even though the monkeys were not rewarded based on the microstimulation, their reports were consistently biased in favor of the direction preferred by the stimulated neurons, strongly suggests that the perceptual consequence of MT microstimulation are similar to the perceptual effects of a visual stimulus moving in the preferred direction. Our goal is to use a similar reward strategy, and test whether we can use optostim

bioRxiv preprint doi: https://doi.org/10.1101/2021.02.16.431182; this version posted February 17, 2021. The copyright holder for this preprint (which was not certified by peer review) is the author/funder. All rights reserved. No reuse allowed without permission.

to affect perception in a predictable way while monkeys perform a challenging visual task and are rewarded solely based on the visual stimulus.

As a first step toward using our toolkit, we focused on the phenomenon of visual masking since it provided us with a simple test of perceptual substitution. The response of neurons in the visual cortex to visual stimuli is highly nonlinear. For example, the response to a stimulus that is at 100% contrast is typically much lower than twice the response at 50% contrast [17]. A perceptual correlate of this neural nonlinearity is visual masking. The threshold for detecting a dim visual target is low on a uniform gray background (**Fig. 1B, top**) and significantly higher when it is added to a co-localized medium brightness pedestal (**Fig. 1B, bottom**), consistent with Weber's law [18].

Here, we used our toolkit to ask three related questions. (1) Can we substitute for a visual pedestal with low-power (<1 mW/mm^2) direct optostim of the visual cortex and cause significant elevation in detection threshold of visual targets? (2) If so, is there a sublinear interaction between visual and optogenetic evoked neural responses in behaving macaque V1 (similar to the sublinearity between a visual pedestal and a visual target) that could account for the behavioral masking effect? (3) What is the spatial specificity of these effects, or in other words, how do the behavioral and neural effects depend on the location of the visual target relative to the receptive fields of the optostimulated neurons?

Results

The overarching goal of the current study was to test two related hypotheses: (i) that low-power optogenetic stimulation (optostim) can substitute for a localized visual mask and cause a significant drop in behavioral detection sensitivities, and (ii) that this perceptual effect is caused by a sublinear interaction between the neural responses elicited in macaque V1 by concomitant visual and direct optogenetic

bioRxiv preprint doi: https://doi.org/10.1101/2021.02.16.431182; this version posted February 17, 2021. The copyright holder for this preprint (which was not certified by peer review) is the author/funder. All rights reserved. No reuse allowed without permission.

stimulation. To test these hypotheses, we developed an optical-genetic toolkit that allowed us to simultaneously measure and stimulate optically neural responses in the cortex of behaving macaques.

An optical-genetic toolkit for reading and writing neural population responses in behaving macaques

Our toolkit employs genetic and optical components. For the genetic component, we used our previously developed methods to express in two macaques at two V1 sites per monkey a calcium indicator (GCaMP6f) in excitatory neurons [13]. After we observed robust visual-evoked GCaMP responses (**Fig. 2C-D**; **Fig. S1 A-C**), we used a second viral vector to express the red-shifted opsin C1V1 in excitatory neurons at a one of the GCaMP expressing sites (**Fig. 2A**)(see Methods). We refer to the site with GCaMP and C1V1 as the "C1V1 site" and the site with GCaMP only as the "GCaMP-only site". We find robust and stable co-expression of GCaMP and C1V1 which lasts for the lifetime of our imaging chambers (>2 years in both chambers; **Fig. 2D**; **Fig. S1 A-C**).

Second, in order to image visual and optogenetic evoked GCaMP responses, we modified our widefield fluorescent imaging system to include an optical stimulation path (**Fig. 2B**). Even though the stimulation light covered both sites, optostim driven responses could only be measured at the C1V1 site (**Fig. 2C, bottom**). This confirms that optical stimulation light (at 580 nm) was efficiently blocked from contaminating our GCaMP imaging measurements (see Methods). Using this system, we can measure responses to visual stimulation, to optostim, and to the combination of the two. Pilot imaging experiments revealed robust GCaMP responses to optostim at peak power densities below 1 mW/mm^2 that were within the ballpark of the visual-evoked responses. Therefore, for monkey L, we chose to test the behavioral and neural effect of optostim at peak power levels of 0.6 and 1.2 mW/mm^2 (**Fig. 2C**). To image the calcium signals we excited GCaMP molecules with blue light (at 480 nm). Pilot detection experiments revealed that, due to the broad excitation spectra of C1V1 [14], the blue GCaMP excitation light can affect the monkey's detection performance. We therefore minimized the blue light level to ~0.01mW/mm^2 by

bioRxiv preprint doi: https://doi.org/10.1101/2021.02.16.431182; this version posted February 17, 2021. The copyright holder for this preprint (which was not certified by peer review) is the author/funder. All rights reserved. No reuse allowed without permission.

running the camera at a low frame rate (20 Hz) and at very low saturation level (see Methods). At this low light level, we did not observe any perceptual effects of blue light illumination. Therefore, under the conditions tested here, the cross-talk between the optical "read" and optical "write" components in our system is negligible.

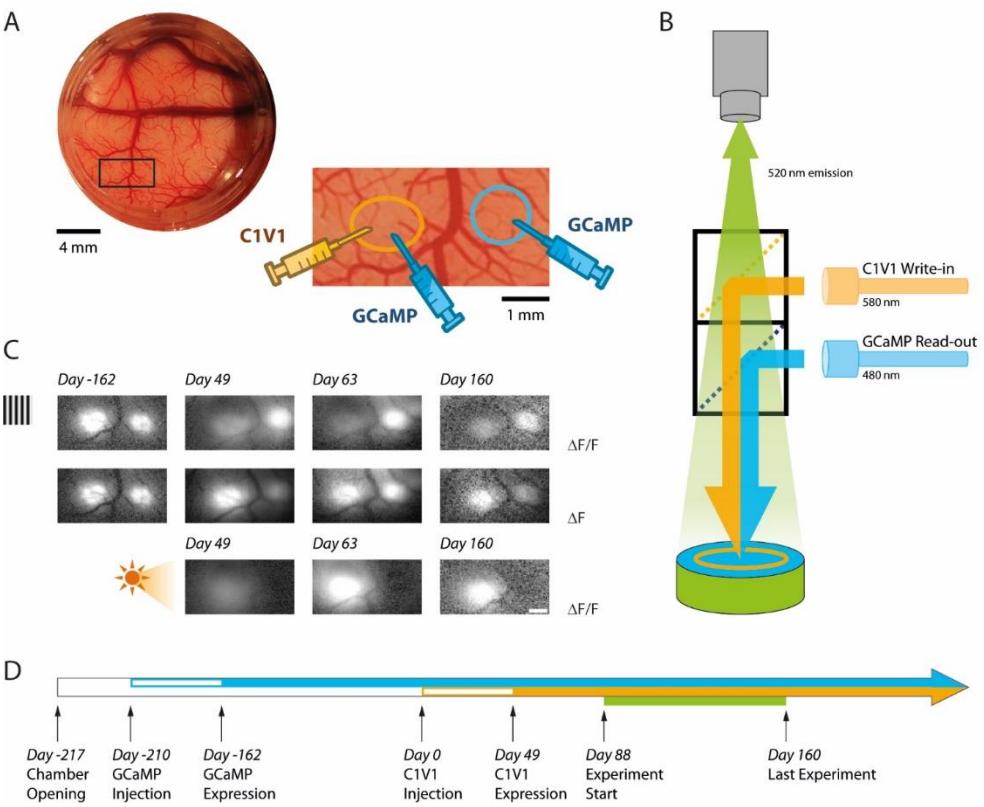

Figure 2. Simultaneous calcium imaging and optostim in V1 of monkeys performing a visual detection task. (A) Top left: picture of cranial window over macaque V1 in Monkey L seen through the artificial dura, with a region of interest indicated by the black rectangle. Bottom right: the zoomed in region encompasses two nearby injection sites of viral vectors that are about 3 mm apart (~0.6° separation between the corresponding receptive fields). The vector carrying the transgene for the calcium indicator GCaMP6f was injected at both sites. The vector carrying the transgene for the opsin C1V1 was only injected at the site on the left after GCaMP expression was verified (**panel C, top**). We refer to the site with GCaMP and C1V1 as the "C1V1-site" and the site with GCaMP only as the "GCaMP-only" site. **(B)** Schematic diagram of our combined imaging and optostim setup. To image the calcium indicator GCaMP6f signals, the cortex is illuminated through a dichroic mirror with blue light (480 nm). Green

bioRxiv preprint doi: https://doi.org/10.1101/2021.02.16.431182; this version posted February 17, 2021. The copyright holder for this preprint (which was not certified by peer review) is the author/funder. All rights reserved. No reuse allowed without permission.

fluorescent signals reflecting increase in intracellular calcium concentration due to neural activity are collected by a sensitive sCMOS camera. To stimulate the red-shifter opsin C1V1, orange light (580 nm) is reflected to the cortex through a second dichroic mirror. The blue and orange lights are blocked from the camera by the dichroic mirrors and an emission filter so that the camera only collects the green fluorescent signals. Notes that imaging was performed simultaneously at both sites and that light stimulation covered both sites. **(C)** Response maps for visual and optostim in monkey L at different time points. A large visual grating evoked a GCaMP response at both sites (top and middle rows). When expressed as $\Delta F/F$ (top row), visual-evoked response at the C1V1 site were weaker following C1V1 expression due to increase baseline fluorescence from the eYFP that is attached to the C1V1 (see Methods). When considering ΔF (middle row), the response evoked by the visual stimulus is comparable at the two sites. Optostim with photostimulation covering both locations elicits a strong GCaMP response at the C1V1 site and little or no response at the GCaMP-only site (bottom row). **(D)** Timeline of GCaMP and C1V1 viral injections, first detection of expression, and behavioral experiments in monkey L.

Low-power optostim in macaque V1 causes a large and selective behavioral masking effect

To test the hypothesis that low-power optostim can substitute for a visual mask and cause a significant decrease in neural and behavioral detection sensitivities, we trained two macaque monkeys to perform a reaction-time visual detection task (**Fig. 1C**). A visual target (a small white Gaussian stimulus; 0.33° FWHM) appeared at a known location on half of the trials. To receive a reward, the monkey had to indicate the presence of the target by making a saccade to the target location on target-present trials, or to maintain fixation if the target was absent (see Methods). In separate blocks, we measured the monkeys' ability to detect the visual target with no optostim (**Fig. 1C, top right**) and when optostim was applied *in all trials* (**Fig. 1C, bottom right**). Note that in the optostim blocks, optostim acted as a visual pedestal (**Fig. 1B, bottom**) and the monkey had to discriminate between trials with optostim only and trials in which the visual stimulus and optostim input coincided. Optostim was applied in 5 ms pulses at 44 Hz; optostim onset was delayed 40 ms relative to visual target onset to compensate for the latency of the visual

bioRxiv preprint doi: https://doi.org/10.1101/2021.02.16.431182; this version posted February 17, 2021. The copyright holder for this preprint (which was not certified by peer review) is the author/funder. All rights reserved. No reuse allowed without permission.

responses so that response onset to the visual target and to optostim coincided; optostim offset matched visual target offset; **Fig. 1C right**; see Methods).

If low-power optostim and visual stimuli activate separate neural populations in V1, or if they combine additively in the same population, then we might expect the optostim pedestal to have little or no perceptual masking effects. On the other hand, if the responses to visual and optostim interact sublinearly in V1 (as do the responses to two superimposed visual stimuli; **Fig. 1B, bottom**), we would expect low-power optostim to cause a significant increase in the monkeys' detection threshold relative to the no optostim blocks. Consistent with the second hypothesis, we found that optostim caused a large perceptual masking effect that led to a reduction in the monkey's ability to detect the visual target in the presence of optostim (**Fig. 3**). Across all experiments in monkey L, optostim at 0.6 mW/mm^2 caused a large and significant drop in the monkey's accuracy (**Fig. 3C**) and a corresponding increase in detection threshold (**Fig. 3D**). In this monkey, optostim caused primarily a large drop in hit rate (**Fig. 3A**) and much smaller increase in false alarm rate (one minus correct rejections rate)(**Fig. 3B**). Increasing the optostim peak power density to 1.2 mW/mm^2 caused a further decrease in accuracy and increase in detection threshold. In addition to a significant increase in detection threshold, optostim also caused a significant reduction in the monkey's detection criterion at the higher power density (**Fig. 3E**). This could reflect incomplete adjustment of the internal criterion used by the monkey for reporting the presence of the target. In other words, the results suggest that the criterion adjustment failed to fully compensate for the perceptual consequences of the optostim.

A similar large perceptual masking effect of optostim was observed in monkey T (**Fig. 3F-H,I-J**). Because the behavioral effects of optostim at 0.6 mW/mm^2 were already high, we also tested the effect of optostim at 0.3 mW/mm^2. Even at this low power level, we observed a significant increase in detection threshold in the presence of optostim. In this monkey, optostim caused mainly an increase in the false alarm rate and a smaller drop in hit rate, and a significant reduction in the monkey's detection criterion.

bioRxiv preprint doi: https://doi.org/10.1101/2021.02.16.431182; this version posted February 17, 2021. The copyright holder for this preprint (which was not certified by peer review) is the author/funder. All rights reserved. No reuse allowed without permission.

Thus, our results reveal that low-power optostim in macaque V1 can substitute for a visual mask and cause large behavioral masking effects.

In contrast to the large and significant effect of optostim on the monkey's detection performance, effect of optostim on the monkey's reaction times were weak and variable (**Fig. S3**).

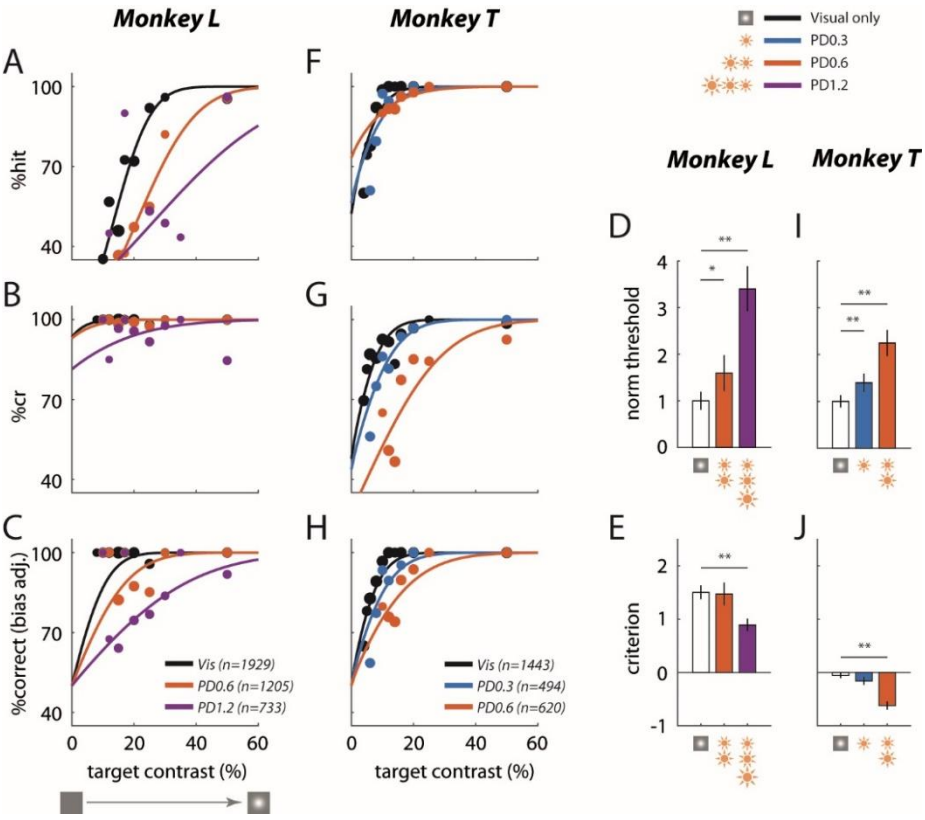

Figure 3. Low power optogenetic stimulation leads to a large behavioral masking effect in a visual detection task. Summary of behavioral performance as a function of target Weber contrast at the C1V1 site for Monkey L **(A-E)** and monkey T **(F-J)**. Performance is broken down into: **(A) "**hits" - target present trials correctly identified, and **(B)** "correct rejections" or "cr" - target absent trials correctly identified. **(C)** Detection performance corrected for the animal's decision bias (imbalance between hits and correct rejections). The solid lines plot the fitted psychometric curves (see Methods for fitting details). Data were pooled across all visual only experiments and across all experiments of the same optostim peak power density (PD) level (in mW/mm^2). The total number of trials pooled

bioRxiv preprint doi: https://doi.org/10.1101/2021.02.16.431182; this version posted February 17, 2021. The copyright holder for this preprint (which was not certified by peer review) is the author/funder. All rights reserved. No reuse allowed without permission.

for each group is indicated in the legend, and the size of the plotted markers represents the relative number of trials executed at each target contrast. **(D)** Detection threshold with optostim (at 69% correct) plotted relative to the visual target only threshold. **(E)** Criterion bias by each optostim power level. Criterion is reported in d' units from the optimal criterion (criterion = 0), with positive values representing bias towards choosing target absent. Error bars in **(D)** and **(E)** indicate bootstrapped standard deviation (number of bootstrap runs = 1000) of the detection threshold and criterion respectively. **(F)-(J)** are same as **(A)-(E)** for Monkey T's C1V1 site. Asterisks mark statistically significant changes from visual only behavior (* - $p < 0.05$; ** - $p < 0.01$; bootstrapped paired difference).

If the effect of optostim is similar to the effect of a visual pedestal, we would expect the behavioral effect to be selective to visual targets that fall in the receptive field of the C1V1 expressing neurons. Alternatively, if the optostim acts as a general distracter, we may obtain a similar behavioral effect even when the target falls at nearby locations. We repeated the experiments while presenting the target at a location in the visual field that corresponds to the receptive field of the neurons at the GCaMP-only site (distance from visual field location corresponding to the C1V1 site: 0.6° in monkey L and 0.7° in monkey T; recall that optostim light covered both the C1V1 and the GCaMP-only sites). In contrast to the large effects of optostim at the C1V1 site, optostim had a much smaller effect when the target was presented at visual-field location corresponding to the GCaMP-only site (**Fig. 4 A-J**). These results show that the behavioral effect of optostim is spatially selective, consistent with the hypothesis that optostim is acting as a visual mask rather than as a general distracter.

bioRxiv preprint doi: https://doi.org/10.1101/2021.02.16.431182; this version posted February 17, 2021. The copyright holder for this preprint (which was not certified by peer review) is the author/funder. All rights reserved. No reuse allowed without permission.

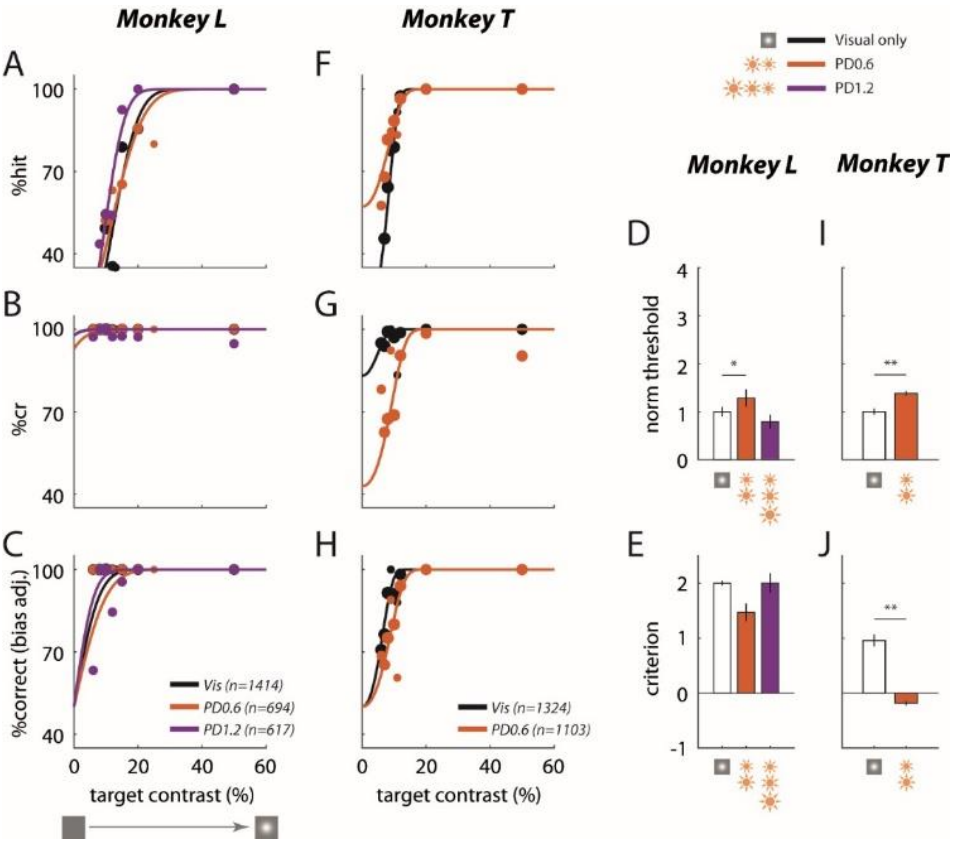

Figure 4. Behavioral effect of optostim is spatially selective. Same as Fig. 3 but at GCaMP-only site.

Sublinear interactions between visual and optostim evoked neural responses in V1 can explain the behavioral masking effects

Our next goal was to use the "reading" component of our optical-genetic toolkit to determine whether a neural correlate of the behavioral masking effect can be observed in macaque V1. While the monkeys performed the detection task, we measured V1 GCaMP responses to the visual stimuli with and without concomitant optostim. **Fig. 5** shows results from two experiments in monkey L when the target was presented at the visual field location corresponding to the C1V1 site. In the first experiment, both the visual target (at 50% Weber contrast) and direct optogenetic stimulation produced similar amplitude responses (**Fig. 5A,B**; the ratio of response to optostim and visual stim at 50% contrast, R_{opto}/R_{vis50}=0.95). The response was stronger when the visual stimulus and the optostim pedestal were presented

bioRxiv preprint doi: https://doi.org/10.1101/2021.02.16.431182; this version posted February 17, 2021. The copyright holder for this preprint (which was not certified by peer review) is the author/funder. All rights reserved. No reuse allowed without permission.

simultaneously (**Fig. 5C**), but the visual-evoked response in the presence of the optostim pedestal was significantly reduced (**Fig, 5D**), consistent with the hypothesis that these two signals interact sublinearly in V1. The time course of the responses reveals similar latency (note that optostim started 40 ms after visual stimulus onset), and a clear reduction in the visual-evoked response in the presence of the optostim baselines (**Fig. 5E;** compare black curve to dashed orange curve). Finally, to measure the overall reduction in the visual-evoked responses in the presence of the optostim, we computed the average visual-evoked response with and without optostim at 5 target amplitudes (**Fig. 5F**; see Methods). Optostim caused a large reduction in the visual-evoked responses at all target amplitudes (average reduction of 50.4%).

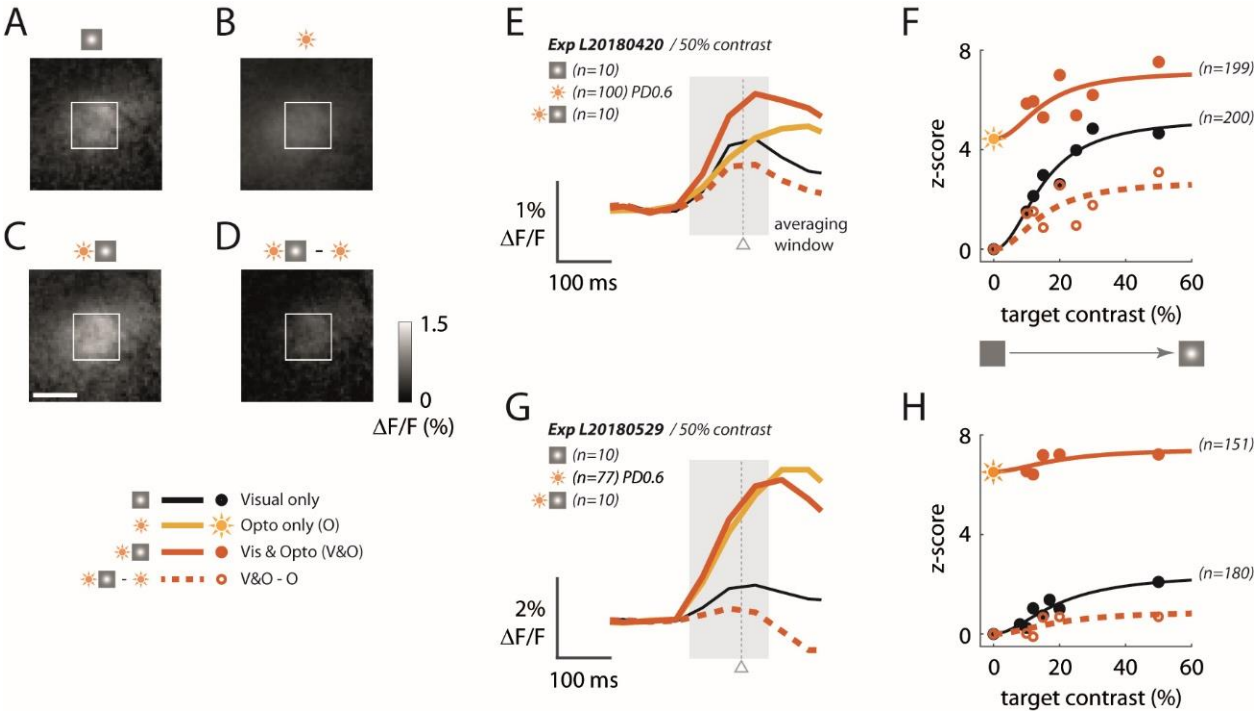

Figure 5. Sublinear neural interactions between visual and optogenetic stimulation in macaque V1 consistent with the behavioral masking effect. (A-D) GCaMP imaging response maps from an example experiment in Monkey L's C1V1 site to **(A)** the visual target alone at 50% Weber contrast, **(B)** optostim alone at PD of 0.6 mW/mm^2, and **(C)** concomitant visual and optostim. **(D)** Visual-evoked response in the presence of optostim (the concomitant response in **(C)** with the optostim baseline response **(B)** subtracted). The white rectangle marks 1x1 mm ROI of cortex selected by maximizing the encompassed visual-only response. The white scalebar marks 1 mm. For **(A-D)**, response was

bioRxiv preprint doi: https://doi.org/10.1101/2021.02.16.431182; this version posted February 17, 2021. The copyright holder for this preprint (which was not certified by peer review) is the author/funder. All rights reserved. No reuse allowed without permission.

averaged over the interval 50 to 200 ms (shaded area in **(E)**). **(E)** Time course of the GCaMP response averaged within the 1x1 mm window as marked in **(A-D)**. The gray triangle indicates the median (saccade) reaction time across all optostim and visual only trials in this experiment. **(F)** Contrast response functions with and without optostim. Each data point is the time-averaged response expressed as a z-score obtained by normalizing with the standard deviation of the blank (no visual and no optostim) trials. Traces indicate the Naka-Rushton curves fitted to the data (see Methods for details). Sun symbol represents response to optostim when target contrast is zero – i.e., response to optostim alone. **(G-H)** are the same as **(E-F)** for a 2nd experiment from Monkey L taken about 6 weeks after the experiment in **(A-D)**. In this experiment, the optostim-evoked response was much larger than the visually-evoked response. See **Fig. S1D** for time course of R_{opto}/R_{vis50} as a function of the day from C1V1 injection in both monkeys.

In a second experiment taken 4 weeks later, the optostim at the same power level produced a response that was much larger than the visual-evoked response (**Fig. 5G**; R_{opto}/R_{vis50}=3.11), suggesting a possible increase in the C1V1 expression level between these two experiments (see **Fig. S1 D** for time course of R_{opto}/R_{vis50}). Consistent with higher level of C1V1, the reduction of the visual-evoked response in the presence of optostim was also larger (**Fig. 5H**), leading to almost complete elimination of the visual-evoked responses in the presence of the optostim pedestal. Similarly, the behavioral effect of optostim in the second experiment (64% increase in detection threshold) was larger than in the 1st experiment (35% increase in detection threshold).

A summary of the physiological results (**Fig. 6**) reveals a strong masking effect of optostim on V1 responses, which is even stronger in monkey T, where even the lowest power level of 0.3 mW/mm^2 almost abolished all visual-evoked GCaMP responses (**Fig. 6C-D**). Separating the results from monkey L to early and late experiments is consistent with significant increase in C1V1 expression level during the course of the experiment (**Fig. S2**) while in monkey T the results appear to be more stable and consistent with the longer delay between C1V1 injections and experiment onset in monkey T (**Fig. S1A, D**).

bioRxiv preprint doi: https://doi.org/10.1101/2021.02.16.431182; this version posted February 17, 2021. The copyright holder for this preprint (which was not certified by peer review) is the author/funder. All rights reserved. No reuse allowed without permission.

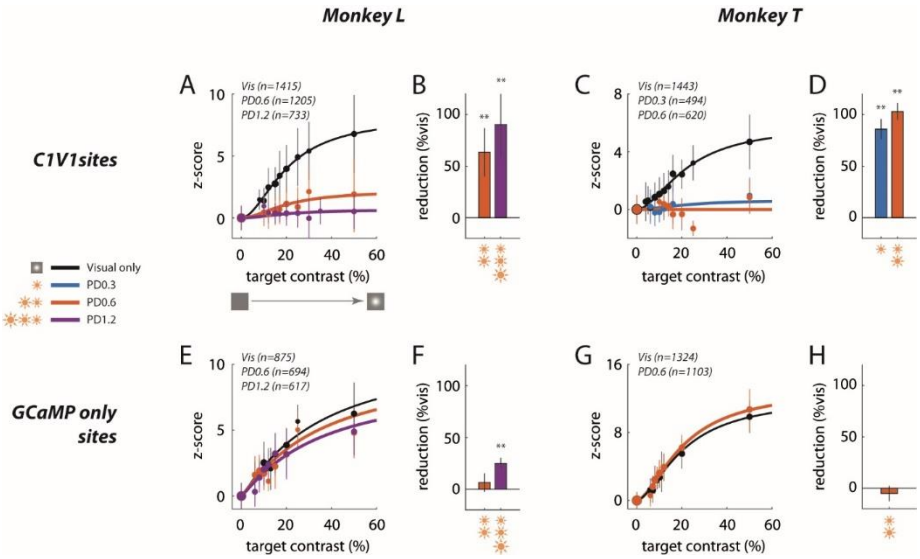

Figure 6. Summary of sublinear interaction between visual and optogenetic stimulation in macaque V1. (A) Contrast response functions for the visual target alone and for the visual target in the presence of optostim (i.e., visual and optostim minus optostim alone) for Monkey L at the C1V1 site. Response in z-score (as in Fig. 5F and H) were pooled across all visual only experiments and across all optostim experiment by the power density (PD) level (in mW/mm^2), matching the plotted data in Fig. 3. The total number of trials pooled for each group is indicated in the legend, and the size of the plotted markers represent the relative number of trials executed at each target contrast. Error bars represent the standard deviation across trials. Traces indicate the Naka-Rushton curve fitted to the data (see Methods for details). **(B)** Monkey L's overall reduction in contrast response function due to optostim relative to the visual only response levels at the C1V1 site. Error bars plot the bootstrapped standard deviation (number of bootstrap runs = 1000). **(C-D)** Same as **(A-B)** for Monkey T's C1V1 site. **(E-H)** are the same as **(A-D)** for respective Monkeys at the GCaMP only sites. Asterisks marks statistical significance of signal reductions using bootstrap analysis.

Finally, to test for the physiological specificity of the nonlinear interaction, we imaged V1 responses at the control GCaMP-only site (**Fig. 6E-H**). We find little or no effect of optostim on the visual-evoked response at the GCaMP-only site even though we could still measure a weak optostim-evoked response (average R_{opto}/R_{vis5o}=0.33 at this site). This weak optostim response could reflect a mixture of direct optogenetic

bioRxiv preprint doi: https://doi.org/10.1101/2021.02.16.431182; this version posted February 17, 2021. The copyright holder for this preprint (which was not certified by peer review) is the author/funder. All rights reserved. No reuse allowed without permission.

activation of horizontal axons originating from the C1V1 site and reaching the GCaMP only site and/or spread of neural responses elicited by optogenetic stimulation at the C1V1 site through horizontal connections. Future studies with more focal activation of either site would allow one to estimate the contribution of these two possible sources. Overall the observed physiological specificity is consistent with the specificity of the behavioral effect (**Fig. 4**).

Discussion

We report here the first use of our optical-genetic toolkit for bi-directional probing of the visual cortex in behaving macaques. We used a viral based method to stably co-express in excitatory neurons the calcium indicator GCaMP6f, for optically "reading" neural population responses at one wavelength, and the red-shifted opsin C1V1, for simultaneously optically "writing" neural responses at a different wavelength. We then developed a single-photon (widefield) optical system capable of simultaneously reading and writing neural population responses while monkeys perform a demanding visual detection task.

We used our toolkit to test the hypothesis that low-power (peak power density <1 mW/mm^2) direct optostim of the visual cortex can recapitulate the perceptual masking effect of a visual pedestal on visual detection (i.e., Weber's law), and that this perceptual masking effect is due to sublinear interaction between visual and optogenetic evoked neural responses in behaving macaque V1 (similar to the nonlinearity between two superimposed visual stimuli).

We found that monkeys' detection thresholds are significantly elevated when the visual target is presented simultaneously with low-power optostim. Concurrent optostim and GCaMP imaging revealed that the decline in behavioral detection sensitivity could be attributed to sublinear interaction between the optogenetically and visually driven neural responses in V1; i.e., responses evoked by the visual target decrease significantly when riding on top of an optostim-driven response pedestal. Finally, we find that

bioRxiv preprint doi: https://doi.org/10.1101/2021.02.16.431182; this version posted February 17, 2021. The copyright holder for this preprint (which was not certified by peer review) is the author/funder. All rights reserved. No reuse allowed without permission.

these neural and behavioral masking effects are spatially selective. The effects are maximal when the target is at the visual field location corresponding to the receptive field of the stimulated neurons, and become weak when the stimulus is moved to a nearby location.

Most previous detection experiments in NHPs that have used optostim were designed to reward the animal for reporting the optostim signal (e.g., [4,19]). In contrast, an important feature of our experiment was that the animals were rewarded to report only the visual stimulus, and were thus incentivized to ignore the optostim signal. If the neural representations of the visual stimulus and the optogenetic-evoked response were distinct and separable, we would have expected the monkeys to learn to effectively ignore the optostim and perform the task with similar accuracy in blocks with and without optostim. Our finding that monkeys show large and consistent perceptual masking effects of optostim, indicates that the optostim evoked response is largely inseparable from the visual evoked response, and that optostim can substitute for a visual stimulus even when the animal is motivated to ignore it. The finding that the perceptual effect is specific to the case where the visual stimulus and optostim activate the same neurons in V1 suggests that optostim is acting as a visual pedestal.

Our experimental approach builds on our ability to maintain, for extended periods (typically > 2 years), cranial windows with direct optical and physical access to the cortex of awake, behaving macaques. This approach has multiple advantages. For example, it allows us to perform viral injections under visual guidance and to monitor in real-time the viral spread [19], to use imaging to confirm the GCaMP and opsin expression in parallel and across multiple injections sites, to monitor the long-term stability of the expression, and to calibrate the stimulation parameters based on the optically measured neural responses. One weakness of the current opsin construct is that the eYFP tag that is attached to C1V1 creates a fluorescent baseline that reduces the functional GCaMP signal (**Figs. 2C, S1C**). Future use of an opsin with a red static fluorescent tag will address this issue.

bioRxiv preprint doi: https://doi.org/10.1101/2021.02.16.431182; this version posted February 17, 2021. The copyright holder for this preprint (which was not certified by peer review) is the author/funder. All rights reserved. No reuse allowed without permission.

Relevance for sensory cortical neuroprostheses

Our results have important implications for the development of future optical brain-computer interfaces (oBCI; [20]). First, while previous results suggest that virally delivered genes can lead to stable foreign protein expression for extended periods in human and non-human primates, we document here stable co-expression of reporters and actuators for periods that exceed the lifespan of our chambers (typically > 2 years; monkey T's chamber is still active more than 30 months from chamber opening with continued stable expression of GCaMP and C1V1; **Fig S1**), and possibly for the lifespan of the animal.

Second, effective optostim at low power densities is important for stable, long-term use in future implantable oBCIs. Behavioral and physiological effects of optogenetics in macaques typically require high stimulation light power densities (e.g., [8-10]), leading to concerns about possible tissue damage [21] and reduced effectiveness of optostim over time. High light level may also limit the use of future implantable devices due to power requirements. We demonstrate that very low optical power levels are sufficient to elicit reliable neural responses within the biologically relevant dynamic range of neural responses to visual stimuli, and to replace a visual mask with optostim in a visual detection task. In fact, the optostim power densities reported here overestimate the actual effective power densities used in our study. Because the optostim light was flashed with a duty cycle of 22%, the time-average of the power density was only a fraction of the maximum power density reported. Preliminary results suggest that the optostim evoked neural response are proportional to the time-average of the power density of the light stimulation and are insensitive to the temporal parameters of the stimulation (**Fig S5**). In addition, we used orange light at 580 nm to stimulate C1V1 in order to prevent the optostim light from contaminating our concomitant calcium imaging. This orange light is shifted from the peak excitation of C1V1 (~530 nm) and this further reduced the effective power of the optostim.

bioRxiv preprint doi: https://doi.org/10.1101/2021.02.16.431182; this version posted February 17, 2021. The copyright holder for this preprint (which was not certified by peer review) is the author/funder. All rights reserved. No reuse allowed without permission.

Nonlinear interaction between visual and direct optostim response in macaque V1

Our results reveal clear sublinear interaction between neural responses elicited by visual stimuli and by direct optogenetic stimulation in V1. While it is well known that neural responses to visual stimuli are highly nonlinear and are consistent with luminance and contrast gain control (e.g., [17, 22]), some of the nonlinearities observed in V1 response are likely to be inherited from its ascending inputs. It is therefore unclear how much of the gain control is implemented in V1 and whether the interactions between visual and optostim evoked responses are similar to those evoked by two visual stimuli. Our results reveal a significant contribution of V1 circuits to gain control, or normalization.

The observed sublinear interaction between visual and optogenetic-evoked responses in V1 is consistent with recent findings from a study using electrophysiology and optogenetics in fixating macaque V1 [9]. However, in that study, the light power densities required to elicit responses were one to two orders of magnitude larger than in the current study, and despite these high power densities, optogenetic-evoked responses were typically much smaller than visual evoked responses, in contrast to our results (e.g., **Fig. 5G-H; Fig S1**). Multiple factors could contribute to the different sensitivity to optostim, including differences in opsin expression levels, differences in the size of the neural population stimulated and/or monitored in the two studies, and difference in the visual stimulus (drifting gratings vs. a small Gaussian target in the current study).

Our results contrast with those of a recent study which used optostim and electrophysiology to examine the perceptual and neural effect of V1 optostim in monkeys performing detection of very dim visual gratings on a dark background (more than two orders of magnitude darker than in the current study) [12]. In that study, optostim caused a small *improvement* in detection when stimulus orientation was near the preferred orientation of the optostimulated neurons, but had no effect when it was far. Electrophysiological measurements revealed no interaction between average visual and optogenetic

bioRxiv preprint doi: https://doi.org/10.1101/2021.02.16.431182; this version posted February 17, 2021. The copyright holder for this preprint (which was not certified by peer review) is the author/funder. All rights reserved. No reuse allowed without permission.

evoked responses, but instead, optostimulation induced a reduction in noise correlations between pairs of neurons only when stimulus orientation was near the preferred orientation of the optostimulated neurons. These contrasting results are not surprising given that the two studies examined the interactions between visual and optogenetic stimulation under very different regimes of cortical activity.

Low-power optostim-evoked responses exceed responses to the visual stimulus

We find that even though optostim engages gain control mechanisms in V1, low-power optostim can elicit GCaMP population responses that far exceed the responses to our Gaussian targets (**Fig. 5G,H; Fig. S1D**). This is an interesting observation, but it does not necessarily imply that optostim can drive V1 population responses to a range that exceeds the population response to any visual stimulus. First, even for the small Gaussian stimuli used in the current study, it is likely that population responses can increase significantly by increasing the target amplitude while lowering the background luminance. Because the background luminance in the current study was high relative to the target amplitude, the response evoked by our Gaussian targets was moderate.

Second, it is possible that other classes of visual stimuli can elicit population responses that are higher than the response to a Gaussian target. However, we recently found that localized low spatial frequency stimuli are surprisingly effective at driving V1 population activity [23]. Widefield calcium imaging signals at each cortical location reflect the weighted sum of neural activity pooled over a Gaussian shaped region with a space constant of ~0.2 mm [19, 24]. Therefore, the GCaMP evoked neural response reflects the pooled spiking activity of a large population of neurons with diverse tuning properties. The Gaussian stimuli used here are suboptimal for individual V1 neurons because they are unoriented. Even though they drive individual neurons weakly, they can lead to robust population response in V1 because they activate a large fraction of the neurons at the corresponding retinotopic location. In contrast, visual stimuli that are optimized for a subset of V1 neurons, such as oriented Gabor patches, activate strongly a small

bioRxiv preprint doi: https://doi.org/10.1101/2021.02.16.431182; this version posted February 17, 2021. The copyright holder for this preprint (which was not certified by peer review) is the author/funder. All rights reserved. No reuse allowed without permission.

subpopulation but activate poorly most other neurons. Therefore, Gaussian targets could be surprisingly effective at driving locally pooled V1 population responses. Consistent with this possibility, detection thresholds for Gaussians are comparable to detection thresholds for Gabor patches [25].

The relative range of population responses achievable by direct optogenetic stimulation of excitatory V1 neurons vs. visual stimuli is an important question for future research. If future results reveal that optostim of excitatory neurons can drive V1 population responses outside of the range achievable with visual stimuli, such a result could reflect several causes. One possibility is that optostim does not engage gain control to the same extent as visual stimuli because during visual responses V1 receives ascending inputs that have already undergone through gain control mechanisms in the retina and LGN. A second possibility is that optogenetic stimulation can partially override gain control mechanisms that operate within V1.

Larger optostim masking effect on V1 neural detection sensitivity than on behavioral sensitivity

Our results reveal larger masking effect of optostim on V1 neural sensitivity than on behavioral sensitivity. In both monkeys, low-power optostim can effectively erase the visual evoked responses from our GCaMP measurements (i.e., reduce target evoked responses by 100%; **Fig. 6B,D**), yet both monkeys could still perform the detection task with optostim (albeit with elevated thresholds). These results suggest that our widefield GCaMP imaging is not capturing all of the visual signals that are available for detection in V1. This could reflect target-evoked signals that are deeper in the cortex and are therefore inaccessible to widefield imaging, visual responses that spread laterally over a larger region than the area affected by optostim, or detection-related signals that bypass V1. In addition, it is possible that even within the affected region, some target-related signals that are present at the single neuron level are eliminated by the indiscriminate pooling of widefield imaging over large populations of neurons.

bioRxiv preprint doi: https://doi.org/10.1101/2021.02.16.431182; this version posted February 17, 2021. The copyright holder for this preprint (which was not certified by peer review) is the author/funder. All rights reserved. No reuse allowed without permission.

Future directions

While our study and previous findings [9] reveal clear nonlinear interaction between visual and optostim evoked responses in V1, additional research is needed in order to achieve a more complete understanding of these nonlinearities and their underlying mechanisms. Our study demonstrates the importance of combining optogenetic stimulation and optical imaging to calibrate the stimulation so that the evoked neural response falls in a biological-relevant regime. Future studies could take further advantage of this simultaneous read-write capability and use real-time close-loop feedback to optimize the stimulation pattern. In the current study, we used spatially homogeneous optogenetic light stimulation to generate a pedestal of optostim-evoked neural responses. An important future direction is to replace the current source of the optogenetic light stimulation with a projector that would allow one to generate arbitrary spatiotemporal patterns of light stimulation [26, 27], thus furthering the ability to mimic with optostim the pattern of population responses elicited by visual stimuli at relevant topographic scales such as retinotopy and orientation columns. This form of patterned optostim could be used in the future to causally test specific hypotheses regarding the role of topography in sensory cortical representations.

Methods

All procedures have been approved by the University of Texas Institutional Animal Care and Use Committee and conform to NIH standards.

Viral Injection

Two macaque monkeys (monkey L and monkey T; macaca mulatta, male, 7-8 years of age during experimentation, weighing 11 and 7kg respectively) were implanted with a custom recording chamber placed over cranial windows for direct physical and optical access to the awake macaque primary visual cortex (V1; **Fig. 2A; Fig. S1B**).For neural reading, each monkey was first injected with a GCaMP6f [13] viral

bioRxiv preprint doi: https://doi.org/10.1101/2021.02.16.431182; this version posted February 17, 2021. The copyright holder for this preprint (which was not certified by peer review) is the author/funder. All rights reserved. No reuse allowed without permission.

vector [Monkey L with AAV1-CaMKIIa-NES-GCaMP6f (Deisseroth lab), and Monkey T with AAV1-CaMKIIa-GCaMP6f (Zemelman lab)]. Progress of the GCaMP6f expression was monitored by measuring visual response to large gratings flashing at 4 Hz (**Fig. 2C; Fig S1C**). Initial expression of GCaMP6f was observed at around 6-10 weeks post injection. Stable functional response levels were reached 4-8 weeks after (**Fig. 2D; Fig S1 A**) and lasted for the lifespan of the chamber (> 2 years in both monkeys).

For neural writing, following stable GCaMP6f expression, a second viral injection was performed collocated to one of the initial GCaMP6f expression sites. This viral vector contained a red-shifted ChR based opsin C1V1 [14] (AAV5-CaMKIIa-C1V1(t/t)-TS-eYFP (Deisseroth lab) for both monkeys). Progress of the C1V1 expression was monitored by measuring the vector's eYFP static florescence and evoked response of the collocated GCaMP6f expression to direct optical stimulation. Initial C1V1 expression was observed 4-6 weeks post injection, and again took 4-8 weeks for stable functional response levels to be obtained (**Fig. S1**). Because the eYFP emission spectrum overlaps with that of GCaMP, the baseline fluorescence (F) at the co-expression site was significantly elevated after the C1V1 expression, leading to an apparent reduction in the amplitude of the visual-evoked responses at this site relative to the GCaMP only site (**Fig. 1C, top**). However, the change in fluorescence in response to the visual stimulus (ΔF) remained comparable at the two sites (**Fig. 1C, middle**), indicating stable expression of both the GCaMP and C1V1 (see also **Fig. S1C**).

Widefield GCaMP Imaging and Optical Stimulation

The experimental technique for widefield (1-photon) fluorescent optical imaging of neural response in awake-behaving macaques was adapted from previous studies [19, 28]. Briefly, each monkey was implanted with a metal head post and a metal recording chamber located over the dorsal portion of V1 (**Fig. 2A; S1B)**, a region representing the lower contralateral visual field at eccentricities of 2–5°.

bioRxiv preprint doi: https://doi.org/10.1101/2021.02.16.431182; this version posted February 17, 2021. The copyright holder for this preprint (which was not certified by peer review) is the author/funder. All rights reserved. No reuse allowed without permission.

Craniotomy and durotomy were performed. A transparent artificial dura made of silicone was used to protect the brain while allowing optical access for imaging [29].

Widefield optical imaging employed a double-SLR-lens-macro system with housing for dichroic mirrors in between the two SLR lenses (**Fig. 2B**). The combination of a 50 mm fixed-focus objective lens (cortex end, Nikkor 50mm f/1.2) and an 85 mm fixed-focused (Canon EF 85mm f/1.2L USM) camera lens provided 1.7x magnification, corresponding to imaging approximately an 8 x 8 mm^2 area of the cortex (using PCO Edge 4.2 CLHS sCMOS camera).

An appropriate set of interference filters and dichroic mirrors were employed to adapt the system for GCaMP6f imaging. The illumination (excitation) light was filtered at 480 nm (ET480/20x), through a long-pass dichroic mirror at 505nm (505LP), and GCaMP6f emission was filtered at 520 nm (ET520/20m).

To further adapt the apparatus for simultaneous neural reading and writing, a second dichroic box was inserted on the camera side to accommodate the optical stimulation light path. This light path was set up with a filter set for C1V1 excitation at 580 nm (ET580/20x), through a short-pass dichroic mirror at 550 nm (550SP). Additionally, the eYFP static florescence co-expressed with the C1V1 was tracked with a 505 nm excitation filter (ET505/20x), a 455/520/600 nm multiband dichroic (69008BS) and a 540 nm emission filter (ET540/30m). All filter parts were obtained from Chroma.

Illumination for GCaMP read-out was supplied with a broadband LED light source (X-Cite120LED). Optical stimulation was also applied with a broad-spectrum LED light source (X-Cite120LED for monkey L, and X-Cite Xylis for monkey T). Due to overlap between GCaMP6f and C1V1 absorption spectra, it was observed that excessive GCaMP read-out blue illumination can lead to decreased visual target detection rate. Therefore, imaging was conducted with minimal GCaMP illumination power (~0.01mW/mm^2) at a low camera saturation level (1-5%) and a low 20 Hz frame rate.

bioRxiv preprint doi: https://doi.org/10.1101/2021.02.16.431182; this version posted February 17, 2021. The copyright holder for this preprint (which was not certified by peer review) is the author/funder. All rights reserved. No reuse allowed without permission.

Imaging was conducted using software developed in-house running in Matlab R2018b (utilizing Image Acquisition Toolbox). Data acquisition was time locked to the animal's heartbeat (EKG QR up-stroke). Raw images were captured at 2048 x 2048 resolution, binned to 512 x 512. EKG was measured using HP Patient Monitor (HP78352C).

Behavioral Task with Concomitant Optical Stimulation

The monkeys detected a white Gaussian target on a uniform gray background (**Fig. 2C**). The monkeys' performance in blocks of trials with no optostim (**Fig. 1C, top right**) was compared with their performance in blocks of trials in which an optostim "pedestal" appeared on all trials (both target present and absent trials). Note that even in the optostim blocks, the monkeys were rewarded only for reporting the presence or absence of the visual target (**Fig. 1C, bottom right**).

The Gaussian target was small (0.39° FWHM), and was positioned at corresponding retinotopic coordinates of the C1V1 expression site. This was 1.5° eccentricity (-35° from the right-hand horizontal meridian) in Monkey L and was 2.7° eccentricity (-46° from the right-hand horizontal meridian) in Monkey T. For the GCaMP only experiments, the visuals stimulus was centered at the retinotopic location corresponding to a nearby cortical site with only GCaMP6f expression (no C1V1 injection/expression). This was 2.0° eccentricity (-45° from the horizontal meridian) for Monkey L, and 2.0° eccentricity (-40° from the horizontal meridian) for Monkey T.

Each trial began with fixation at the fixation point. An auditory tone and the dimming of the fixation point cued the monkey to the start of the detection task trial. 250 ms later, the Gaussian target was presented on 50% of the trials. The monkeys were trained to stay at the fixation point on target absent trials or make a saccade to and hold gaze (for 150 ms) at the target position to indicate target detection (with a 75 ms minimum allowed reaction time). When the target was present, it remained on screen for a maximum of 250 ms or was extinguished upon the monkeys' saccade (**Fig. 1C right**). The monkey was given 600 ms to

bioRxiv preprint doi: https://doi.org/10.1101/2021.02.16.431182; this version posted February 17, 2021. The copyright holder for this preprint (which was not certified by peer review) is the author/funder. All rights reserved. No reuse allowed without permission.

make the saccade or to hold the fixation point, and was subsequently rewarded on correct choices [stay (correct reject) on target absent trials, and saccade to target (hit) on target present trials].

The strength of the Gaussian target is reported in Weber contrast:

$$c = \frac{L_{max} - L_{background}}{L_{background}}$$

The contrast of the Gaussian target was varied to measure the psychometric curve. Trials were presented in blocks with the target contrast was held constant within each block. Blocks were pooled and the detection threshold was estimated from the monkey's choices by maximum likelihood fitting the following equations for hits and correct rejections:

$$P(HITs) = \Phi\left(\frac{1}{2}\left(\frac{c}{\alpha}\right)^{\beta} - \delta\right), \qquad P(CRs) = \Phi\left(\frac{1}{2}\left(\frac{c}{\alpha}\right)^{\beta} + \delta\right)$$

where Φ is the standard cumulative normal function, α the detection threshold at d-prime (d') = 1, β the steepness of the psychometric curve, and δ the monkey's bias from the optimal criterion (in units of d'). Monte Carlo resampling of trials was used to bootstrap the fitted parameters for statistical analysis.

The monkeys' baseline detection threshold was assessed in blocks of trials with no optostim. In separate blocks on the same day, the detection threshold with optostim was obtained for comparison.

Psychometric curves from visual only and optostim trials were fitted jointly, allowing different thresholds (α) and biases (δ), but sharing the same steepness parameter (β). The change in the behavioral threshold in visual-plus-optostim trials was characterized as the fraction increase of the visual-only threshold:

$$\rho_{behavior} = \frac{\alpha_{optovis} - \alpha_{vis}}{\alpha_{vis}}$$

The visual target was presented 250 ms after the auditory cue, whereas the optostim was applied 290 ms after the cue. This 40 ms delay in optostim insured that optostim-evoked V1 response coincides approximately with the onset of the visual-target-evoked response on target present trials (**Fig. 5E, G**).

bioRxiv preprint doi: https://doi.org/10.1101/2021.02.16.431182; this version posted February 17, 2021. The copyright holder for this preprint (which was not certified by peer review) is the author/funder. All rights reserved. No reuse allowed without permission.

Optostim was presented in pulses of 5 ms spaced every 22.5 ms (~44 Hz), and was extinguished after 210 ms (coinciding with maximum visual target duration) or on the onset of saccade (coinciding with extinguishing the visual target). Pilot studies in which we compared GCaMP response to pulsed and continuous optostim suggest that the V1 response is approximately proportional to the time average of the optostim power density (**Fig. S5**). These pilot studies suggest that the effective power density was about 25% of the peak power density reported here.

The power density of optostim was varied as an experiment parameter. Power density (in mW/mm^2) was measured through all the optical filters/apparatus at the plane of the imaged cortex, with the total power read from a light meter (ThorLabs PM100D with S170C sensor) and divided by the illuminated area (circular disk: diameter 13 mm for C1V1 optostim light, and 19 mm for GCaMP light).

Experiments were conducted with custom code using TEMPO real-time control system (Reflective Computing). The visual stimulus was presented on a Sony CRT (1024x768 @ 100 Hz), distanced 108 cm from the animal (50 pixels-per-degree), with mean luminance 50 cd/m^2. Visual stimulus was generated using in-house real-time graphics software (glib). Eye tracking was implemented with an EyeLink 1000 Plus.

GCaMP Neural Response Analysis

For each trial, an image sequence was captured for a total of 1.2 seconds including pre-stimulus and post-stimulus frames. The image sequence was analyzed to extract the visual and optical stimulation-evoked response using a variant of the previous reported routines [19, 24, 30]. Additional stages were added to the routine to reduce known sources of noise.

The preprocessing stage of image analysis involved the following steps: image stabilization, down-sampling, $\Delta F/F$ normalization, heart-beat removal, and pre-stimulus anchoring. Image stabilization is a

bioRxiv preprint doi: https://doi.org/10.1101/2021.02.16.431182; this version posted February 17, 2021. The copyright holder for this preprint (which was not certified by peer review) is the author/funder. All rights reserved. No reuse allowed without permission.

new routine to de-accentuate blood vessel edges in the ΔF/F response map caused by micro movements of the camera and/or the cortex during imaging.

The image intensity across time at each individual pixel was modelled with separable motion-free ($I_{xy0}[t]$) and motion-related ($\vec{\alpha}_{xy}.\vec{v}[t]$) components as follows:

$$I_{xy}[t] = I_{xy0}[t] + \vec{\alpha}_{xy}.\vec{v}[t]$$

For each trial, a single global motion vector $\vec{v}[t]$ was obtained by estimating the translational motion of the center portion of the images (1/4 of the imaging area). The motion coefficients $\vec{\alpha}_{xy}$ for each pixel was then obtained using least squares fitting to the model. The motion-corrected image is $I_{xy0}[t]$. This approach to image stabilization (compared to traditional image registration approach) has the advantage of correcting for non-rigid movements (rotations, expansion/contractions, affine transformation, local distortions, etc.) and sub-pixel motion.

Heartbeat removal employed a similar approach. The heartbeat artefact is a much larger for imaging in the GCaMP spectrum than for imaging in the voltage-sensitive-dye spectrum. Due to slight differences in heartrate between trials, despite synchronizing imaging start on a QRS upstroke of the EKG, subsequent heartbeats fall on different frames across trials, which lead trial-to-trial variations that cannot be removed with a simple blank-subtraction approach. Nonetheless, the EKG synchronized start of trials acted as a common pivot point across trials, and as the heartrate changed, the heartbeat artefact stretched or compressed in time like an accordion from this pivot. Consequently, the pixel intensities at the same frame index across trials varied in a predictable manner with respect to the heartrate of in each trial. This was exploited in the following model, putting the heartrate-free stimulus-driven response ($S_{xyt}(s)$, to stimulus *s*) and heartrate-related ($f_{xyt}(HR[k])$) intensity values as additive components:

$$I_{xyt}[k] = S_{xyt}(s) + f_{xyt}(HR[k])$$

bioRxiv preprint doi: https://doi.org/10.1101/2021.02.16.431182; this version posted February 17, 2021. The copyright holder for this preprint (which was not certified by peer review) is the author/funder. All rights reserved. No reuse allowed without permission.

where $HR[k]$ is the estimated heartrate on trial k. The heartrate-related component (artefact) was modelled with a fourth-order polynomial of the heartrate:

$$f_{xyt}(HR[k]) = {a_{xyt}}^4 HR^4[k] + {b_{xyt}}^3 HR^3[k] + {c_{xyt}}^2 HR^2[k] + d_{xyt} HR[k]$$

Trials from all stimulus conditions were pulled from the same recording session, from which the heartrate-free stimulus-driven responses and polynomial coefficients were estimated simultaneously using least squares fitting; and then the estimated heartrate-related component was subtracted out from the data.

The measured physiological signal was ΔF/F. For each trial, the average florescence over frames 0 to 150 ms prior to stimulus onset (3 frames [F5-F7]) was used as the baseline reference (F_0). ΔF/F was calculated as follows:

$$\frac{\Delta F}{F}(t) = \frac{F(t) - F_0}{F_0}$$

The neural response was averaged over the 1x1 mm cortical area presenting the best visually driven response. The mean response within this window was taken over time to characterize the time course of the neural response (**Fig. 5E,G**). Slow drifting responses over time were minimized with a linear de-trending routine using the following model of the stimulus driven response ($R_S[t]$) for each stimulus condition *S*:

$$R[t] = R_S[t] + (m_S + m_k).t$$

This model treats the linear trend as two component gradients: a linear trend on the conditional means (m_S) shared across all trials from the same stimulus condition *S*, and additional linear trends in individual trials (m_k). m_k was estimated by minimizing the squared errors within trials for the same stimulus conditions, using the data up to the frame that a saccade was made. Pre-stimulus frames were used to estimate m_S, which constrained all the conditional means ($R_S[t]$) to a flat, zero pre-stimulus baseline. The detrending routine removed both components of the linear trend in the data.

bioRxiv preprint doi: https://doi.org/10.1101/2021.02.16.431182; this version posted February 17, 2021. The copyright holder for this preprint (which was not certified by peer review) is the author/funder. All rights reserved. No reuse allowed without permission.

The average response over the three frames from 50 to 200 ms post-stimulus was used to represent the neural signal pertaining to the animal's behavioral decision. Response beyond this range was not used as they are generally post-saccade (median saccade times were 149 and 204 ms respectively for Monkey L and T; **Fig. S3**). The Naka-Rushton function was used characterize the neural response as a function of visual stimulus contrast (*c*):

$$R(a) = R_{max}\frac{c^n}{c^n + {c_{50}}^n}$$

The contribution of the visually stimulus in concomitant visual and optostim trials (optovis response) was calculated by subtracting the mean optostim only baseline response ($R_{optobase}$) from the concomitant trial response (optosub response):

$$R_{optosub} = R_{optovis} - R_{optobase}$$

The reduction of the visually-evoked response under concomitant optostim was expressed as proportional reduction from the visual-only response:

$$\rho_{physiology} = \frac{R_{vis} - R_{optosub}}{R_{vis}}$$

Monte Carlo resampling of trials was used to bootstrap the reduction distribution for statistical analysis.

The sensitivity measure, z-score values (**Fig. 5F,H; Fig. 6**), were calculated with respect to the standard deviation of the blank (σ_{blank}) (no visual and no optostim) trials:

$$z - score = \frac{R - R_{blank}}{\sigma_{blank}}$$

All analyses were done using Matlab R2018a

Statistics

Two animals were examined to verify consistency of experimental approach and results. Multiple recordings were made from the same animals. The number of recordings were based on previous

bioRxiv preprint doi: https://doi.org/10.1101/2021.02.16.431182; this version posted February 17, 2021. The copyright holder for this preprint (which was not certified by peer review) is the author/funder. All rights reserved. No reuse allowed without permission.

experience; no statistical method was used to predetermine sample size. Where bootstrapped resampling was applied, the data was resampled 1000 times with replacement within trials of the same stimulus condition (visual target amplitude and optostim level). For **Figs. 3, 4** and **Suppl. Fig.. 2**, the behavioral detection threshold and criterion were refitted to each bootstrapped resample of the monkey's behavioral decisions. For **Fig. 6** and **Suppl. Fig. 2**, the GCaMP response reduction were recalculated on each bootstrapped resample of the GCaMP response. Error bars include in the same figures are the standard deviation of the bootstrapped means (equivalent to standard error). Statistical comparisons in **Figs. 3 and 4** are made between bootstrapped distributions, using two-tailed, unpaired Student's t-test. Bootstrapped distributions were assumed to be normal, but this was not formally tested. Statistical analyses were conducted in Matlab (R2018a).

Data and Code Availability

The data and custom code from this study are available from the authors upon reasonable request.

ACKNOWLEDGMENTS

We thank Tihomir Cakic, Kelly Todd, and members of Seidemann laboratory for their assistance with this project. We thank Boris Zemelman for the GCaMP6f viral construct used in monkey T. This work was supported by NIH grants EY-016454 to E.S., EY-024662 to W.S.G. and E.S., BRAIN U01-NS099720 to E.S. and W.S.G., and DARPA-NESD0-N66001-17-C-4012 to E.S.

AUTHOR CONTRIBUTIONS

S.C., G.B., Y.C., E.S. and W.S.G. contributed to the conception, design, interpretation of data, and drafting and revising the article. S.C. carried out the majority of data acquisition and all data analysis. G.B., Y.C.,

bioRxiv preprint doi: https://doi.org/10.1101/2021.02.16.431182; this version posted February 17, 2021. The copyright holder for this preprint (which was not certified by peer review) is the author/funder. All rights reserved. No reuse allowed without permission.

and S.K. assisted in data collection. K.D. and C.R. provided viral vectors for expressing the calcium indicator GCaMP6f and opsin C1V1.

bioRxiv preprint doi: https://doi.org/10.1101/2021.02.16.431182; this version posted February 17, 2021. The copyright holder for this preprint (which was not certified by peer review) is the author/funder. All rights reserved. No reuse allowed without permission.

References

1. Marshel, J.H., Kim, Y.S., Machado, T.A., Quirin, S., Benson, B., Kadmon, J., Raja, C., Chibukhchyan, A., Ramakrishnan, C., Inoue, M., et al. (2019). Cortical layer–specific critical dynamics triggering perception. Science *365*, eaaw5202.

2. Carrillo-Reid, L., Han, S., Yang, W., Akrouh, A., and Yuste, R. (2019). Controlling Visually Guided Behavior by Holographic Recalling of Cortical Ensembles. Cell *178*, 447-457.e445.

3. Dalgleish, H.W.P., Russell, L.E., Packer, A.M., Roth, A., Gauld, O.M., Greenstreet, F., Thompson, E.J., and Häusser, M. (2020). How many neurons are sufficient for perception of cortical activity? eLife *9*, e58889.

4. Ju, N., Jiang, R., Macknik, S.L., Martinez-Conde, S., and Tang, S. (2018). Long-term all-optical interrogation of cortical neurons in awake-behaving nonhuman primates. PLoS Biol *16*, e2005839.

5. Tremblay, S., Acker, L., Afraz, A., Albaugh, D.L., Amita, H., Andrei, A.R., Angelucci, A., Aschner, A., Balan, P.F., Basso, M.A., et al. (2020). An Open Resource for Non-human Primate Optogenetics. Neuron.

6. El-Shamayleh, Y., and Horwitz, G.D. (2019). Primate optogenetics: Progress and prognosis. Proc Natl Acad Sci U S A *116*, 26195-26203.

7. Galvan, A., Stauffer, W.R., Acker, L., El-Shamayleh, Y., Inoue, K.I., Ohayon, S., and Schmid, M.C. (2017). Nonhuman Primate Optogenetics: Recent Advances and Future Directions. J Neurosci *37*, 10894-10903.

8. Ruiz, O., Lustig, B.R., Nassi, J.J., Cetin, A., Reynolds, J.H., Albright, T.D., Callaway, E.M., Stoner, G.R., and Roe, A.W. (2013). Optogenetics through windows on the brain in the nonhuman primate. J Neurophysiol *110*, 1455-1467.

bioRxiv preprint doi: https://doi.org/10.1101/2021.02.16.431182; this version posted February 17, 2021. The copyright holder for this preprint (which was not certified by peer review) is the author/funder. All rights reserved. No reuse allowed without permission.

9. Nassi, J.J., Avery, M.C., Cetin, A.H., Roe, A.W., and Reynolds, J.H. (2015). Optogenetic Activation of Normalization in Alert Macaque Visual Cortex. Neuron *86*, 1504-1517.

10. Jazayeri, M., Lindbloom-Brown, Z., and Horwitz, G.D. (2012). Saccadic eye movements evoked by optogenetic activation of primate V1. Nat Neurosci *15*, 1368-1370.

11. May, T., Ozden, I., Brush, B., Borton, D., Wagner, F., Agha, N., Sheinberg, D.L., and Nurmikko, A.V. (2014). Detection of optogenetic stimulation in somatosensory cortex by non-human primates--towards artificial tactile sensation. PLoS One *9*, e114529.

12. Andrei, A.R., Pojoga, S., Janz, R., and Dragoi, V. (2019). Integration of cortical population signals for visual perception. Nat Commun *10*, 3832.

13. Chen, T.-W., Wardill, T.J., Sun, Y., Pulver, S.R., Renninger, S.L., Baohan, A., Schreiter, E.R., Kerr, R.A., Orger, M.B., Jayaraman, V., et al. (2013). Ultrasensitive fluorescent proteins for imaging neuronal activity. Nature *499*, 295-+.

14. Packer, A.M., Peterka, D.S., Hirtz, J.J., Prakash, R., Deisseroth, K., and Yuste, R. (2012). Two-photon optogenetics of dendritic spines and neural circuits. Nature methods *9*, 1202-1205.

15. Salzman, C.D., Britten, K.H., and Newsome, W.T. (1990). Cortical microstimulation influences perceptual judgments of motion direcion. Nature *346*, 174-177.

16. Salzman, C.D., Murasugi, C.M., Britten, K.H., and Newsome, W.T. (1992). Microstimulation in Visual Area Mt - Effects on Direction Discrimination Performance. Journal of Neuroscience *12*, 2331-2355.

17. Albrecht, D.G., and Hamilton, D.B. (1982). Striate Cortex of Monkey and Cat - Contrast Response Function. Journal of Neurophysiology *48*, 217-237.

18. Cornsweet, T.N., and Pinsker, H. (1965). Luminance discrimination of brief flashes under various conditions of adaptation. The Journal of Physiology *176*, 294.

bioRxiv preprint doi: https://doi.org/10.1101/2021.02.16.431182; this version posted February 17, 2021. The copyright holder for this preprint (which was not certified by peer review) is the author/funder. All rights reserved. No reuse allowed without permission.

19. Seidemann, E., Chen, Y., Bai, Y., Chen, S.C., Mehta, P., Kajs, B.L., Geisler, W.S., and Zemelman, B.V. (2016). Calcium imaging with genetically encoded indicators in behaving primates. eLife *5*.

20. O'shea, D.J., Trautmann, E., Chandrasekaran, C., Stavisky, S., Kao, J.C., Sahani, M., Ryu, S., Deisseroth, K., and Shenoy, K.V. (2017). The need for calcium imaging in nonhuman primates: New motor neuroscience and brain-machine interfaces. Experimental neurology *287*, 437-451.

21. Podgorski, K., and Ranganathan, G. (2016). Brain heating induced by near-infrared lasers during multiphoton microscopy. Journal of Neurophysiology *116*, 1012-1023.

22. Purpura, K., Tranchina, D., Kaplan, E., and Shapley, R.M. (1990). Light adaptation in the primate retina: Analysis of changes in gain and dynamics of monkey retinal ganglion cells. Visual Neuroscience *4*, 75-93.

23. Benvenuti, G., Chen, Y., Ramakrishnan, C., Deisseroth, K., Geisler, W., and Seidemann, E. (2018). Scale-Invariant Visual Capabilities Explained by Topographic Representations of Luminance and Texture in Primate V1. Neuron *100*, 1-9.

24. Chen, Y., Palmer, C.R., and Seidemann, E. (2012). The relationship between voltage-sensitive dye imaging signals and spiking activity of neural populations in primate V1. Journal of Neurophysiology, 3281-3295.

25. Watson, A.B., and Ahumada, A.J. (2005). A standard model for foveal detection of spatial contrast. Journal of vision *5*, 6-6.

26. Huang, X., Elyada, Y.M., Bosking, W.H., Walker, T., and Fitzpatrick, D. (2014). Optogenetic assessment of horizontal interactions in primary visual cortex. J Neurosci *34*, 4976-4990.

27. Chen, Y., Benvenuti, G., Miller, D., Sullender, C., Radaei, F., Dunn, K.A., Ramakrishnan, C., Deisseroth, K., Geisler, W.S., and Seidemann, E. (2019). A bi-directional optical-genetic toolkit for reading and writing topographic neural population codes in behaving macaque cortex. In Soc. for Neuroscience.

bioRxiv preprint doi: https://doi.org/10.1101/2021.02.16.431182; this version posted February 17, 2021. The copyright holder for this preprint (which was not certified by peer review) is the author/funder. All rights reserved. No reuse allowed without permission.

28. Seidemann, E., Arieli, A., Grinvald, A., and Slovin, H. (2002). Dynamics of depolarization and hyperpolarization in the frontal cortex and saccade goal. Science *295*, 862-865.

29. Arieli, A., Grinvald, A., and Slovin, H. (2002). Dural substitute for long-term imaging of cortical activity in behaving monkeys and its clinical implications. Journal of Neuroscience Methods *114*, 119-133.

30. Chen, Y., Geisler, W., and Seidemann, E. (2006). Optimal decoding of correlated neural population responses in the primate visual cortex. Nature Neuroscience *9*, 1412-1420.

bioRxiv preprint doi: https://doi.org/10.1101/2021.02.16.431182; this version posted February 17, 2021. The copyright holder for this preprint (which was not certified by peer review) is the author/funder. All rights reserved. No reuse allowed without permission.

Supplementary Figures

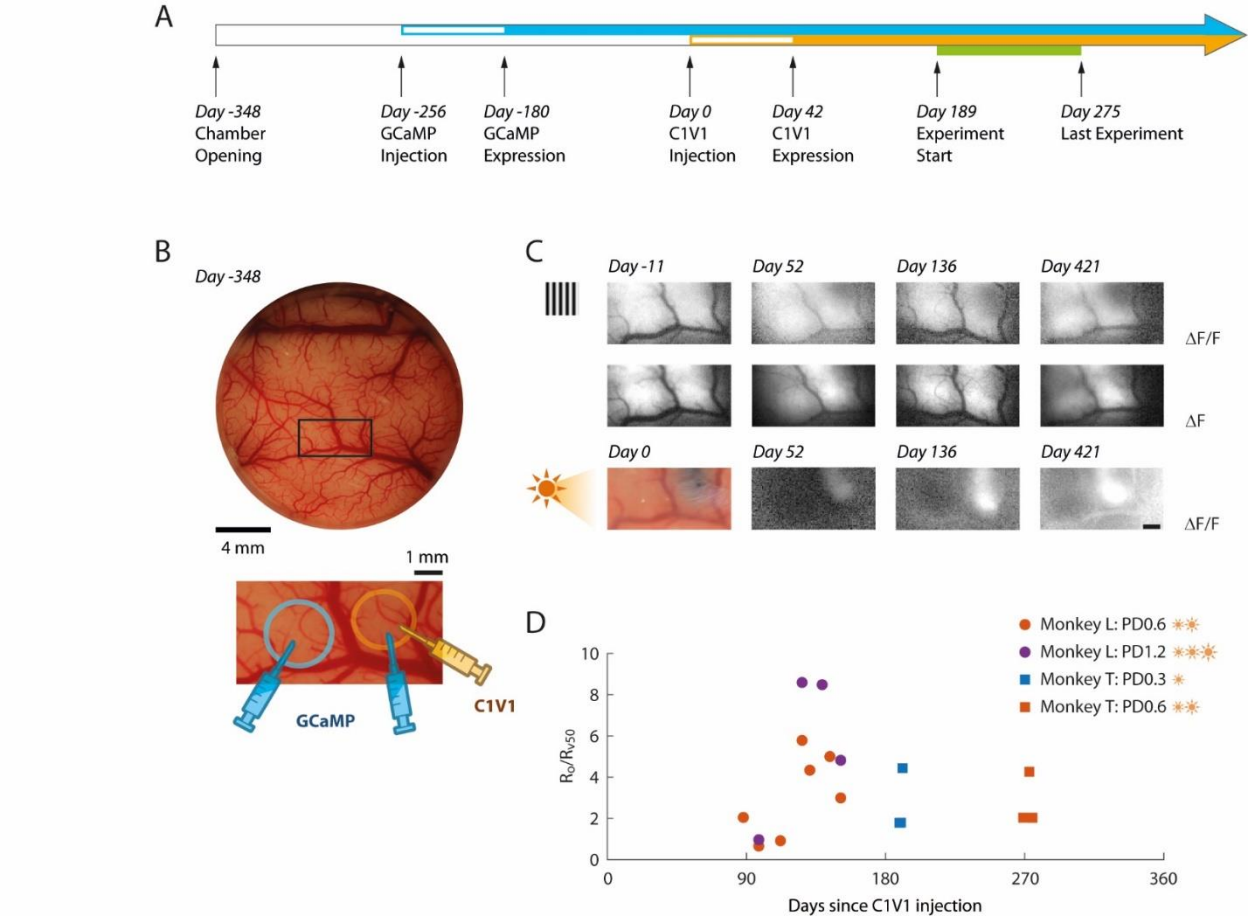

Supplementary Figure 1

Stable expression of GCaMP and C1V1 in monkey T. **(A)** Timeline of GCaMP and C1V1 viral injections, first detection of expression, and behavioral experiments in monkey T. **(B)** Cortical chamber with an ROI encompassing the GCaMP only and C1V1 viral injections sites. For monkey T, these sites are about 4 mm apart (corresponding to ~0.7° separation in the visual field). **(C)** Visual response to a large grating evokes a GCaMP response at both sites before and after C1V1 injection (first and second rows). Optostim with light stimulation at both locations elicits a strong GCaMP response at the site with C1V1 and little or no response at the site with only GCaMP (third row). The photo of the cortex at Day 0 (C1V1 injection)

bioRxiv preprint doi: https://doi.org/10.1101/2021.02.16.431182; this version posted February 17, 2021. The copyright holder for this preprint (which was not certified by peer review) is the author/funder. All rights reserved. No reuse allowed without permission.

shows the blue dye that we co-inject with the viral vector to visualize the injection site. **(D)** Response ratio between the optostim evoked GCaMP response and the response evoked by a 50% contrast Gaussian target (behavioral experiments), plotted against days from C1V1 injection date, for both monkey L and monkey T.

bioRxiv preprint doi: https://doi.org/10.1101/2021.02.16.431182; this version posted February 17, 2021. The copyright holder for this preprint (which was not certified by peer review) is the author/funder. All rights reserved. No reuse allowed without permission.

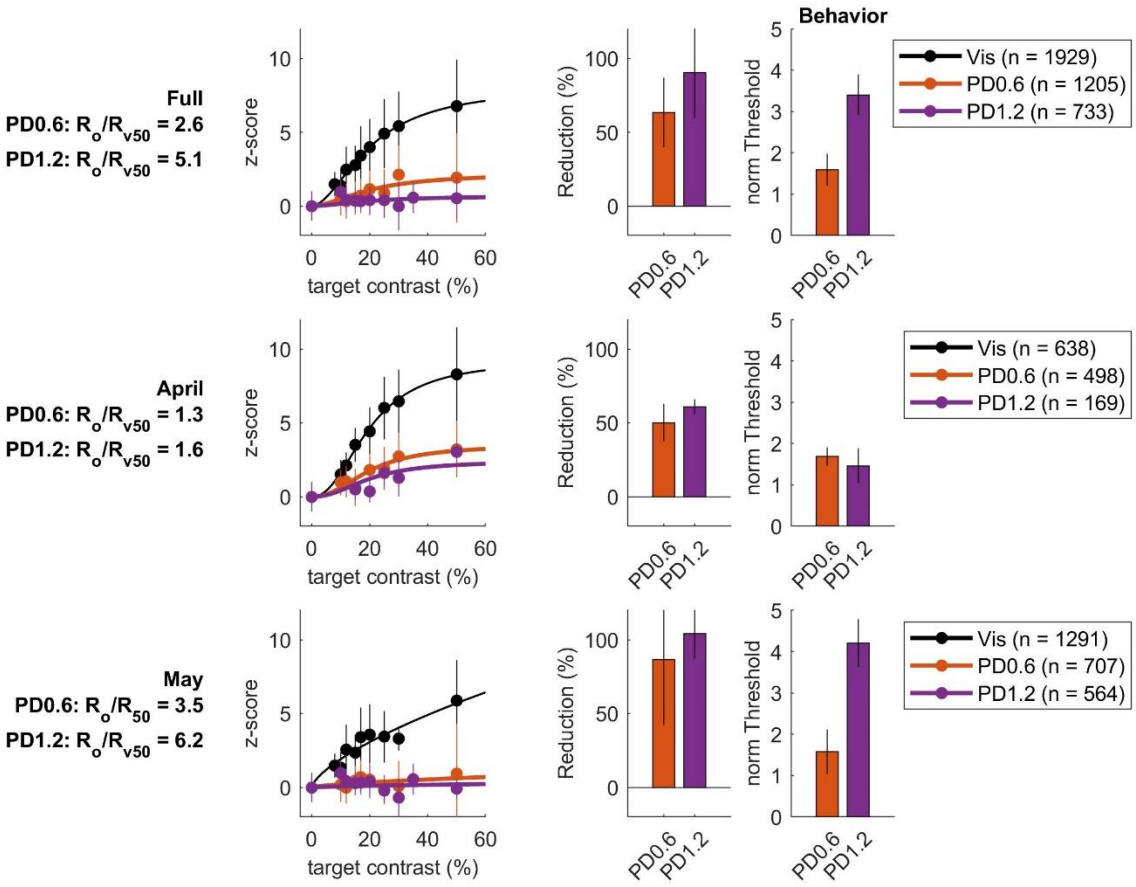

Supplementary Figure 2

Monkey L's physiological (in same format as **Fig. 6**) and behavioral results (as **Fig. 3D**), separated to early (April) and late (May/June) experimental periods. It appears that the C1V1 expression further strengthened between the early and later experimental periods. The optostim to visual only response ratio (R_o/Rv_{50}) increased substantial between the early and late experimental periods.

bioRxiv preprint doi: https://doi.org/10.1101/2021.02.16.431182; this version posted February 17, 2021. The copyright holder for this preprint (which was not certified by peer review) is the author/funder. All rights reserved. No reuse allowed without permission.

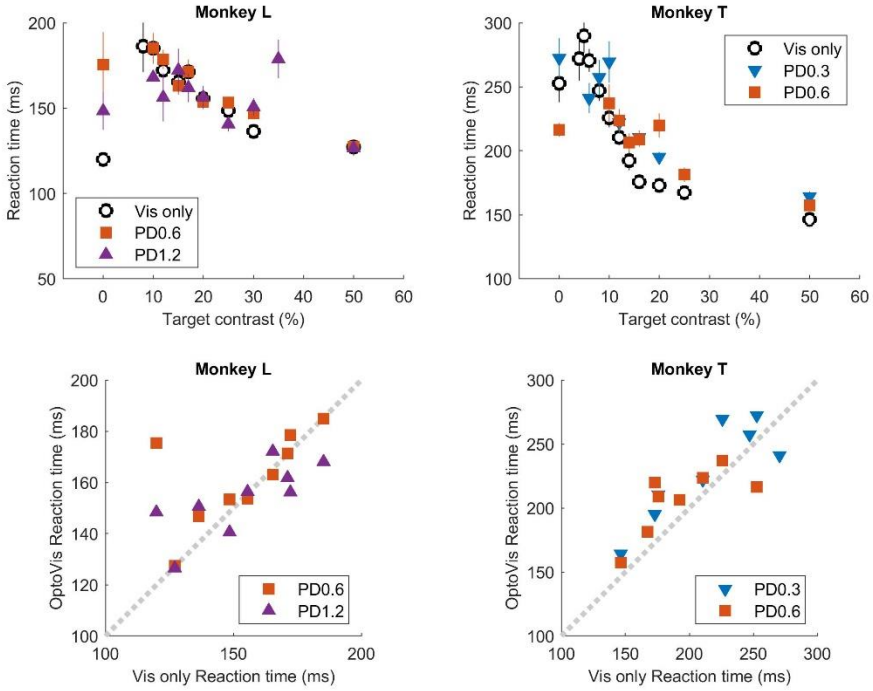

Supplementary Figure 3

Effect of optostim on reaction time. Top row: average reaction time plotted against target contrast for monkey L and monkey T (combined across all experiments). 0% contrast illustrates the average reaction time of false alarms. Error bars indicate s.e.m. Bottom row: reaction time from the optostim block for each target contrast plotted against the reaction time to the corresponding visual only target.

bioRxiv preprint doi: https://doi.org/10.1101/2021.02.16.431182; this version posted February 17, 2021. The copyright holder for this preprint (which was not certified by peer review) is the author/funder. All rights reserved. No reuse allowed without permission.

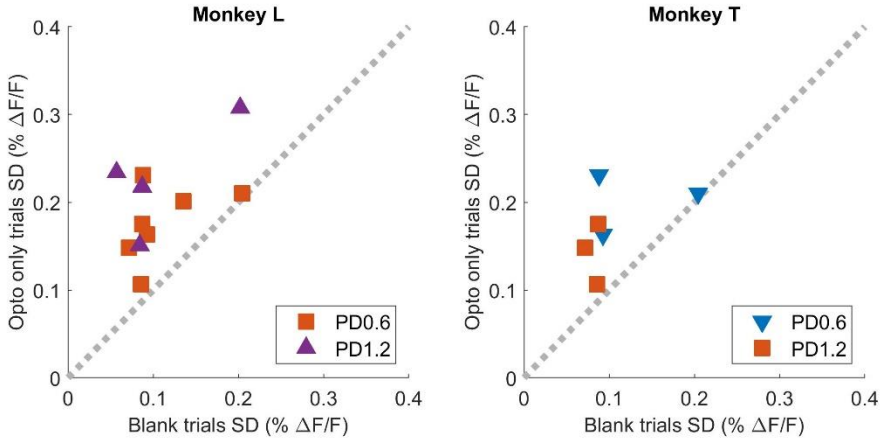

Supplementary Figure 4

Effect of optostim on variability: standard deviation across trials in the optostim block for each target contrast, plotted against that from the corresponding visual only target.

bioRxiv preprint doi: https://doi.org/10.1101/2021.02.16.431182; this version posted February 17, 2021. The copyright holder for this preprint (which was not certified by peer review) is the author/funder. All rights reserved. No reuse allowed without permission.

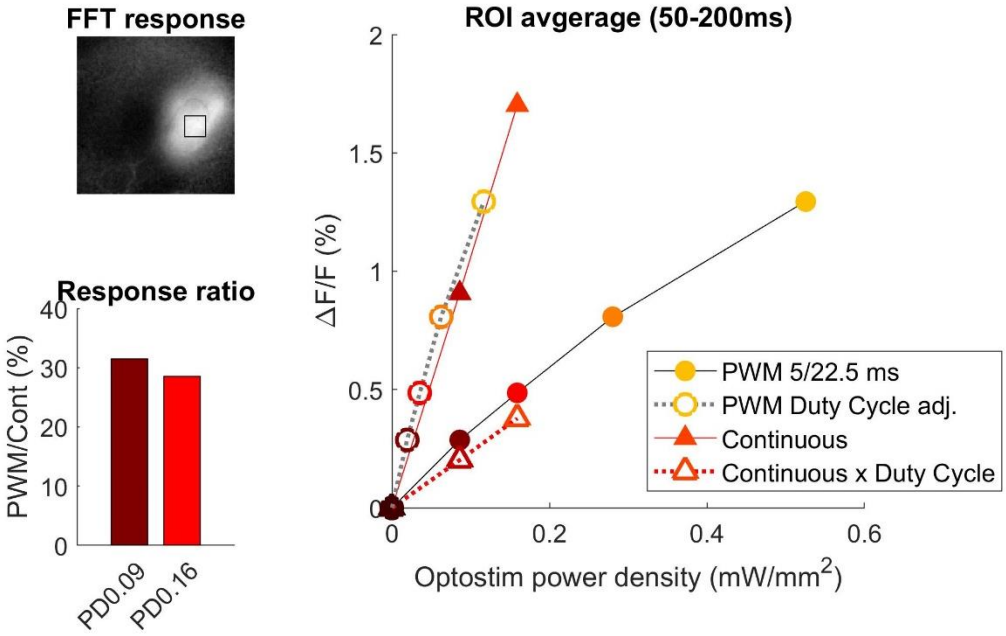

Supplementary Figures 5

Comparison of evoked responses to pulsed (PWM) and continuous optostim. In a separate concomitant GCaMP and C1V1 site in monkey T, the response strength from continuous optostim was compared with the pulsed optostim (5 ms every 22.5 ms cycle) adopted in the main study over a range of optostim power levels. At the same power level setting, the pulsed optostim response (solid circles) was ~30% of the continuous optostim response (solid triangles); the result is similar to that predicted by the pulsed optostim duty cycle (5/22.5 = 22.2%). This equivalence is further illustrated by the open triangles, which plot the continuous optostim response (solid triangles) scaled down by 0.222. Similarly, the open circles replot pulse optostim responses (solid circles) as a function of the effective optostim power (power density x 0.222); the result closely matches the continuous optostim response (solid triangles).